

## Photoinduced stabilization and enhancement of the ferroelectric polarization in $\text{Ba}_{0.1}\text{Sr}_{0.9}\text{TiO}_3/\text{La}_{0.7}\text{Ca}(\text{Sr})_{0.3}\text{MnO}_3$ thin film heterostructures

Y. M. Sheu,<sup>1</sup> S. A. Trugman,<sup>1</sup> L. Yan,<sup>1</sup> C.-P. Chuu,<sup>2</sup> Z. Bi,<sup>1</sup> Q. X. Jia,<sup>1</sup> A. J. Taylor,<sup>1</sup> and R. P. Prasankumar<sup>1</sup>

<sup>1</sup>Center for Integrated Nanotechnologies, Los Alamos National Laboratory, Los Alamos, New Mexico 87545, USA

<sup>2</sup>Institute of Atomic and Molecular Sciences, Academia Sinica, Taipei 10617, Taiwan

(Received 18 December 2012; published 11 July 2013)

An emerging area in condensed matter physics is the use of multilayered heterostructures to enhance ferroelectricity in complex oxides. Here we demonstrate that optically pumping carriers across the interface between thin films of a ferroelectric (FE) insulator and a ferromagnetic metal can significantly enhance the FE polarization. The photoinduced FE state remains stable at low temperatures for over one day. This occurs through screening of the internal electric field by the photoexcited carriers, leading to a larger, more stable polarization state that may be suitable for applications in areas such as data and energy storage.

DOI: [10.1103/PhysRevB.88.020101](https://doi.org/10.1103/PhysRevB.88.020101)

PACS number(s): 77.55.fe, 73.21.Ac, 73.50.Gr, 78.66.–w

The wide variety of applications for ferroelectric (FE) materials<sup>1</sup> has motivated many fundamental studies aimed at controlling their properties, particularly by increasing the FE polarization and its transition temperature  $T_c$ . Arguably the most heavily studied class of ferroelectrics are the perovskite oxides  $\text{ABO}_3$  (e.g.,  $\text{BaTiO}_3$ ), in which the center cation ( $\text{B}^+$ ) is displaced along one direction with respect to the surrounding oxygen octahedron ( $\text{O}^{2-}$ ), resulting in a spontaneous polarization that can be switched with an applied external electric ( $E$ ) field below  $T_c$ . Interest in these materials substantially increased when they were first fabricated in thin film form in the 1980s, since this enabled their integration into semiconductor chips.<sup>1</sup>

Strain can provide an avenue for tuning the properties of thin FE perovskite oxide films by forcing their in-plane lattice constant ( $a_{\text{in}}$ ) to match that of the substrate.<sup>2</sup> For example, in the case of compressive strain on a cubic substrate, elongation along the surface normal (which lowers the symmetry<sup>3</sup>) reduces the number of possible displacement directions to two, resulting in an increase in  $T_c$ .<sup>2-4</sup> The free energy of this system can be represented by a double-well potential (DWP) [Fig. 1(a)], in which the energetically lower potential well is determined by boundary conditions (e.g., strain,  $E$  field, interfacial atomic structure, etc.) that set the direction of  $\text{B}^+$  displacement and thus the FE polarization. However, this displacement is reduced when the FE polarization is terminated at the film interfaces, as this creates a large internal “depolarizing”  $E$  field ( $E_{\text{int}}$ ) pointing in the opposite direction that reduces the remanent polarization ( $P_r$ , the polarization without an external applied  $E$  field).<sup>1,5,6</sup> This can be overcome by adding charge at the interfaces to screen the depolarizing field, allowing  $P_r$  to nearly reach the bulk value.<sup>5</sup>

This fundamental coupling between  $E_{\text{int}}$  and  $P_r$  limits nanoscale device applications since various boundary conditions usually result in incomplete charge screening that is very sensitive to external parameters.<sup>5</sup> Therefore, a substantial portion of current research focuses on obtaining high  $P_r$  at the nanoscale.<sup>2,5,7,8</sup> This would, for example, increase the contrast between “ON” and “OFF” states in data storage applications.

In this context, it is surprising that relatively little work has explored the use of optical methods for enhancing  $P_r$ ,<sup>10</sup> particularly when an FE film is combined with another

complex oxide film in a multilayered structure to provide additional functionality. One of the most straightforward ways to optically enhance ferroelectricity would be to photoexcite carriers that screen  $E_{\text{int}}$ . However, in individual FE films, electron-hole recombination limits the carrier lifetime, minimizing this enhancement.<sup>10,11</sup> This could be overcome by using a bilayered heterostructure, in which one species of photoexcited carrier (e.g., holes) is isolated on the non-FE side of the interface and the other species (e.g., electrons) is isolated in the FE film, minimizing recombination. This would result in physically separated, long-lived screening charges, potentially leading to high  $P_r$ .

In this Rapid Communication we demonstrate a noncontact, all-optical method for writing and reading the FE polarization in  $\text{Ba}_{0.1}\text{Sr}_{0.9}\text{TiO}_3$  (BSTO) thin films that are grown on ferromagnetic (FM) metallic manganite thin films on different substrates. The lattice mismatch between BSTO and the manganite layers fully strains the BSTO films, giving rise to higher FE  $T_c$ s than in the bulk. More importantly, by photoexciting the manganite films at 1.59 eV, we were able to enhance  $P_r$  through charge transfer across the BSTO/manganite interface, as revealed by detecting the second-harmonic generation (SHG) signal at 3.18 eV, proportional to the FE polarization in BSTO.<sup>9</sup> We observe that this new state has a very long lifetime (over one day) after removal of the initial photoexcitation, suggesting that growth of FE/manganite bilayers offers a new avenue for optically increasing and stabilizing FE order.

Our SHG experiments are based on an amplified Ti:sapphire laser system, using a single laser beam at 1.59 eV to generate SHG from BSTO at 3.18 eV. The standard laser fluence used is  $F_0 \sim 0.25 \text{ mJ/cm}^2$ . The samples used are 50 nm thick BSTO films grown by pulsed laser deposition on 50 nm thick optimally doped manganite films [ $\text{La}_{0.7}\text{Ca}_{0.3}\text{MnO}_3$  (LCMO) or  $\text{La}_{0.7}\text{Sr}_{0.3}\text{MnO}_3$  (LSMO)], using MgO or  $\text{SrTiO}_3$  (STO) (001) substrates. More detail on our experimental setup and sample fabrication is given in the Supplemental Material.<sup>9</sup>

The structural properties of our samples were then determined by x-ray diffraction (XRD) (Fig. 2 table inset). In the 10% Ba-doped STO films studied here, previous work revealed that above 0.2% in-plane compressive strain, the resulting elongation along the surface normal causes a transition to a

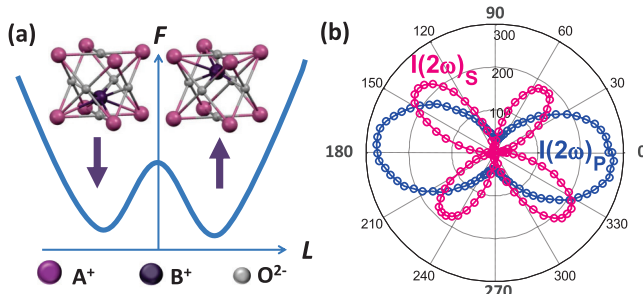


FIG. 1. (Color online) (a) DWP energy ( $F$ ) as a function of  $B^+$  ion ( $Ti^{4+}$  in BSTO) displacement in the FE tetragonal structure. (b) Polar plot of the SHG signal in BSTO/LCMO/MgO, originating from the  $C_{4v}$  symmetry, detected for both  $s$  and  $p$  polarizations. The light is incident at  $\sim 23^\circ$  with respect to the sample normal. More details of the measurement geometry are given in the supplementary material.<sup>9</sup>

tetragonal structure below 75 K,<sup>4</sup> in which the FE polarization either points up or down along the  $c$  axis (associated with tetragonal  $C_{4v}$  symmetry) [Fig. 1(a)]. In our samples, XRD shows that the small bulk lattice mismatch between LC(S)MO and STO strains the LC(S)MO films, matching the  $a_{in}$  of STO. The lattice mismatch between LC(S)MO and MgO is much larger, so that the LC(S)MO/MgO films are relaxed. Furthermore, all BSTO layers are compressively strained to match the  $a_{in}$  of LC(S)MO (Fig. 2 table inset) and thus have a tetragonal structure<sup>2</sup> at room temperature. This is far above previously measured FE  $T_c$ s for single crystals or thick films, which are typically  $\sim 70$ – $80$  K (e.g.,  $T_c \sim 75$  K for a 10% Ba-doped BSTO single crystal).<sup>4,12,13</sup> However, this does not necessitate the existence of a room temperature FE phase in our films, as discussed below.<sup>2,3</sup>

We measured the  $s$  and  $p$  polarized SHG signals in reflection as a function of incident light polarization [Fig. 1(b)], confirming the  $C_{4v}$  symmetry for all of our samples.<sup>9,14</sup> We also performed experiments on individual manganite films to verify the negligible contribution to the SHG signal from LC(S)MO. Figure 2(a) displays the temperature dependence of the SHG signal for all four of the samples studied here with

both fundamental and SHG light  $p$  polarized (abbreviated  $p_{in}$ ,  $p_{out}$ ), which is the configuration that consistently gives the largest SHG signal for all samples. The intersection of the two different slopes in the data indicates  $T_c$ ,<sup>2</sup> below which the tetragonal  $c$  axis contracts upon heating. We find that  $T_c$  is highest in the BSTO/LCMO/MgO sample, consistent with the fact that the BSTO layer is under the highest strain. The variation in  $T_c$  for the other samples with comparable strain values is likely due to the complexity of the phase diagram for BSTO in this strain range, particularly for low Ba doping.<sup>4</sup> This makes  $T_c$  very sensitive to other factors, such as the high photoinduced carrier concentrations discussed below.

Figure 2(b) shows the main result of this work, which is our striking observation of a slow increase in the SHG signal from the BSTO/manganite heterostructures that nearly saturates after tens of minutes.<sup>9</sup> This phenomenon has the following main features in common for all of our heterostructures: (a) As the laser beam moves to a new spot, the entire process repeats, with the SHG signal increasing with time for all BSTO/manganite bilayers. (b) The saturated signal is much larger at low temperatures than at high temperatures [Fig. 2(b)], especially below  $T_c$  in each film. (c) SHG saturation is suppressed in pure BSTO films grown directly on STO or MgO substrates, and the magnitude of the initial SHG signal in pure BSTO is somewhat smaller than that in BSTO/manganite heterostructures. (d) The time scale required to reach saturation is different at each temperature. (e) The long time required to reach saturation at  $F_0$  can be circumvented when a much stronger fluence is used before the sample is saturated [pink curve in Fig. 2(b)]. When comparing signals from samples that have undergone this treatment, the SHG is always detected at  $F_0$ . (f) The SHG signal has a strong correlation with  $T_c$ : the higher  $T_c$ , the higher the SHG signal, both initially and in the saturated state. (g) The SHG symmetry [Fig. 1(b)] does not change with time; only the intensity varies with time. Saturation of the SHG signal is observed in any configuration of fundamental and SHG polarizations, as long as there is a detectable SHG signal. (h) The saturation is suppressed and the high SHG signal disappears when the sample is exposed to air, both of which recur when the sample is returned to vacuum.

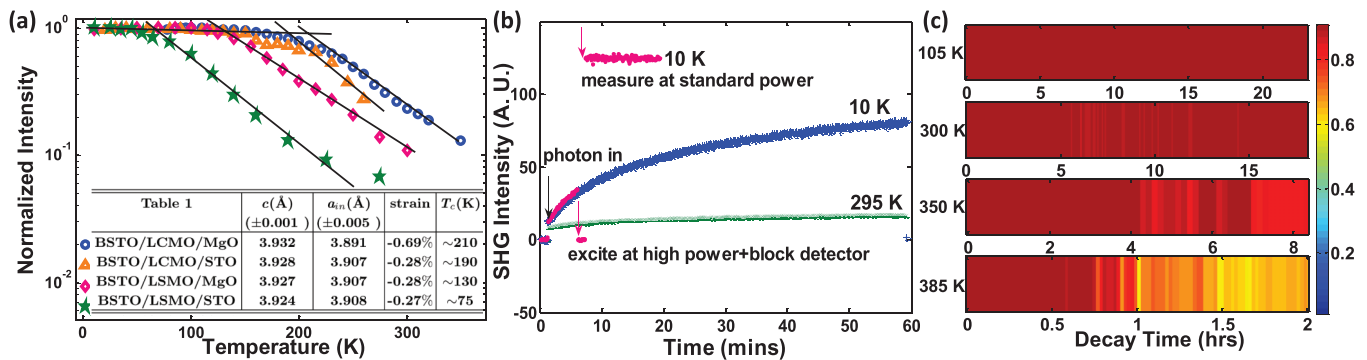


FIG. 2. (Color online) (a) SHG intensity of various films measured for  $(p_{in}, p_{out})$ . Each data set is normalized to its individual signal at 10 K. The table in the inset lists the out-of-plane ( $c$ ) and in-plane ( $a_{in}$ ) lattice constants, the in-plane strain, and  $T_c$  of BSTO on various LC(S)MO/substrate combinations, calculated from XRD. (b) Time-varying SHG signals in BSTO/LSMO/MgO at low and high temperatures. More details are given in the supplementary material.<sup>9</sup> (c) Decay of the SHG signal measured at various temperatures after saturation upon removal of photoexcitation.

Another noteworthy result from our measurements is the extremely long decay time of the photoinduced saturated state. There is no observable decay for over one day at low temperatures [upper panel of Fig. 2(c)] after saturation is reached and the laser beam is blocked (only unblocking it to sample the SHG signal). After a day with no discernible decay we moved the beam to a fresh spot, after which it repeated the saturation process. When we moved the beam back to the original spot, the SHG signal returned with the same intensity. The SHG signal only decays at higher temperatures ( $>300$  K), with a time constant of  $\sim 3$  h at 385 K [lower panel of Fig. 2(c)] that decreases with increasing temperature.

All of the above phenomena are robustly reproducible. Similar saturation phenomena were previously studied in Si/SiO<sub>2</sub>,<sup>15–17</sup> although the dependence on temperature, power, and critical film thickness, as well as the decay time, conflict with our data, and therefore will not be discussed further here.

To explain our observations, we first note that this complex time-varying phenomenon is likely related to photoinduced charge transport across the interface between BSTO and LC(S)MO since it is suppressed in a pure BSTO film and LC(S)MO alone does not contribute to our SHG signal. We can support this hypothesis by estimating the photoinduced interface charge density  $\sim 5 \times 10^{13}$  cm<sup>-2</sup>, assuming that 10% of the pump light is absorbed in LC(S)MO near the interface. This corresponds to a polarization ( $P = Q/A$ , where  $Q$  is the charge and  $A$  is the area of the laser spot) of  $\sim 8$   $\mu\text{C}/\text{cm}^2$  in the saturated state. The overall  $\sim 500$ – $800\%$  increase in SHG intensity from the initial state to the saturated state at 10 K [Fig. 2(b)] corresponds to a  $\sim 200$ – $300\%$  enhancement in the FE polarization, indicating that the initial  $P_r \sim 2$ – $4$   $\mu\text{C}/\text{cm}^2$ . This is comparable to previously reported values for  $P_r$  both near this Ba concentration<sup>12</sup> and at higher concentrations,<sup>18–22</sup> validating our hypothesis that the polarization enhancement is linked to the photoinduced interface charge density.

We can draw additional conclusions from the above considerations. For example, the long-lived nature of the photoinduced state suggests that recombination of the photoexcited carriers is negligible. Furthermore, the strong effect of air exposure on the observed phenomena indicates involvement

of the BSTO surface charge. In addition, ferromagnetism in the LC(S)MO layers does not appear to influence the observed phenomena on the time scales discussed here. Finally, the lack of variation in the SHG polar pattern with time demonstrates that the symmetry of BSTO remains the same upon photoexcitation, indicating that the observed slow increase in the SHG signal is due to further displacement of the Ti<sup>4+</sup> ions along the tetragonal axis.

Overall, these considerations suggest that the photoinduced enhancement of the FE polarization is associated with charge screening at the BSTO surface and BSTO/LC(S)MO interface that compensates the  $E_{\text{int}}$  originating from FE dipoles, making further displacement of Ti<sup>4+</sup> energetically favorable. We note that expansion of BSTO along its tetragonal axis could also lead to an increase in the Ti<sup>4+</sup> displacement and consequent increase in the SHG signal. However, photoinduced heating in LC(S)MO causes the tetragonal axis of BSTO to contract below  $T_c$ .<sup>2</sup> Similarly, photoinduced expansion in the  $ab$  plane of LC(S)MO (which is less likely due to substrate clamping) will cause the  $c$  axis of BSTO to contract, and thus cannot explain our observations.

Based on the above considerations, we provide a phenomenological model to explain the mechanism, neglecting more complex interfacial effects such as band bending and hybridization between Mn and Ti atoms. We begin by microscopically examining the photoinduced charge transfer across the interface. Figure 3(a) displays a schematic band diagram of the interface between insulating BSTO and metallic LC(S)MO. Conduction in LC(S)MO originates from Mn(3d) electrons, while the gap in BSTO is between valence O(2p) states and conduction Ti(3d) states (with a band gap of  $\sim 3.3$ – $3.9$  eV<sup>9,27–31</sup>). Our XRD data indicates that the Ti<sup>4+</sup> and Mn<sup>3+</sup> ions are under compressive and tensile strain, respectively, causing the doublet  $e_g$  and triplet  $t_{2g}$  levels associated with both ions to split.<sup>26</sup> In the FE phase of BSTO the resulting elongation of the  $c$  axis splits the Ti  $t_{2g}$  states into a doublet ( $d_{xz}, d_{yz}$ ) and a singlet  $d_{xy}$ , stabilizing the Jahn-Teller (J-T) distortion, which is specifically sensitive to the strain [Fig. 3(b)].<sup>26</sup> Photoexciting the system at 1.59 eV, which is smaller than the band gap of BSTO but larger than the band offset between the BSTO conduction band and the LC(S)MO

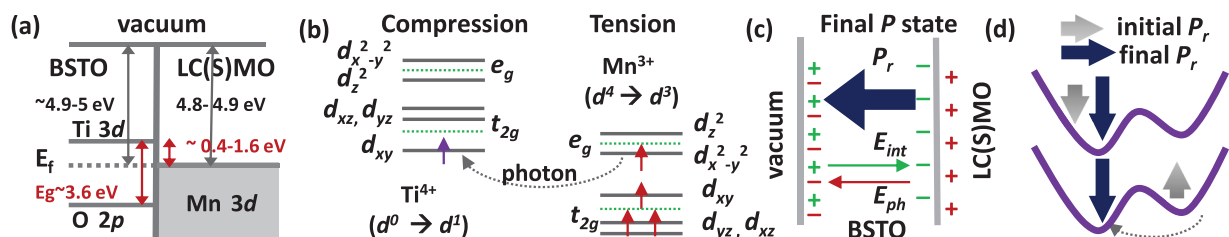


FIG. 3. (Color online) (a) Schematic band diagram of the BSTO/LC(S)MO interface.<sup>9,23–25</sup> (b) Diagram of (tetragonal) crystal field 3d orbital occupation in Ti<sup>4+</sup> and Mn<sup>3+</sup> under compressive and tensile strain, respectively. The green dashed lines depict degenerate levels before they are split by the crystal distortion. Before photoexcitation, Ti<sup>4+</sup> has an empty  $d$  orbital while Mn<sup>3+</sup> has three electrons that half fill the  $t_{2g}$  orbital and one electron that occupies an  $e_g$  orbital.<sup>26</sup> Optical excitation promotes one electron across the interface from Mn<sup>3+</sup> to Ti<sup>4+</sup>, stabilizing the J-T distortion. (c) After photoexcitation,  $e_{\text{ph}}$  propagate towards the BSTO surface, leaving holes behind at the LC(S)MO interface. Green charges represent the initial FE polarization, and red charges represent photoexcited carriers (creating  $E_{\text{ph}}$ ) that screen  $E_{\text{int}}$ , enhancing  $P_r$ , and configuring the final polarization to point towards the BSTO surface. (d) The final  $P_r$  is set by photoexcited carriers that unbalance the DWP energy in the same way, favoring one polar direction irrespective of the initial direction.

Fermi level [Fig. 3(a)],<sup>9</sup> transfers one electron from the  $e_g$  level in LC(S)MO across the interface to occupy the  $Ti^{4+} d_{xy}$  level, changing its valence to  $Ti^{3+}$  and further favoring the J-T distortion.

If these photoexcited electrons ( $e_{ph}$ ) remain near the interface, they will quickly recombine with the photoexcited holes ( $h_{ph}$ ). This can be avoided if the static FE polarization points towards the BSTO surface, as  $E_{int}$  (pointing in the opposite direction) will cause  $e_{ph}$  to move towards the BSTO surface (hopping between nearest neighbor empty Ti  $d$  orbitals, similar to mobile photoexcited electrons in semiconductors), while  $h_{ph}$  remain in LC(S)MO near the interface. These photoexcited charges will then compensate the static FE dipoles at both interfaces, reducing  $E_{int}$  and enhancing the FE polarization [Fig. 3(c)].

In fact, even if the static FE polarization initially points towards the BSTO/LC(S)MO interface, we expect that the final  $P_r$  will point towards the BSTO surface. This can be seen by considering the photoinduced changes in the DWP. The separation of  $e_{ph}$  and  $h_{ph}$  across the interface produces a large interfacial electric field ( $E_{ph} \gg E_{int}$ ) directed towards the BSTO surface, which acts like an applied  $E$  field that unbalances the DWP energy [Fig. 3(d)] and displaces  $Ti^{4+}$  ions towards the surface, causing  $P_r$  to point in that direction. We note that this also happens above  $T_c$ , although the saturated SHG signal is much smaller [Fig. 2(b)] due to the decrease in charge capacity from electron-hole recombination at the interface.

Further support for this mechanism comes from noting that holes in LC(S)MO cannot cross the interface, as this would require one electron to move from BSTO to LC(S)MO, which is not possible since the  $Ti^{4+} d$  orbital is empty and the BSTO O( $2p$ ) states are too far away in energy [Fig. 3(a)].<sup>25</sup> If  $h_{ph}$  move away from the interface into LC(S)MO, then the energy required to sustain their separation from the  $e_{ph}$  is greater than that gained through compensation of the BSTO surface charge. Photoexcited holes can thus minimize their energy by remaining at the interface.

Our results also suggest that the higher  $T_c$ s measured in our samples [Fig. 2(a)] as compared to previous work in which the strain was varied<sup>4</sup> are associated with the screening of  $E_{int}$  by photoexcited carriers. Similarly higher  $T_c$ s were previously observed in  $BaTiO_3$  films sandwiched between metallic electrodes,<sup>2</sup> even though the magnitude of the strain was similar to that in a single film. The reason for the higher  $T_c$ s observed in that work was not given; however, our work indicates that it likely originates from screening by carriers in the metal electrodes.<sup>6</sup>

In summary, using an optical-write SHG-read technique, we created an enhanced polarization state that remains stable for over one day in BSTO/LC(S)MO heterostructures. The magnitude of the estimated initial and final remanent polarization agrees with previously reported values. The ON and OFF processes initiated through photoexcitation in vacuum and through exposure to air, respectively, open up the possibility of noncontact optically controlled data storage. Future work on decreasing the response time will be critical in optimizing these heterostructures for such applications. In addition, the long-lived photoinduced FE state stores photoexcited carriers by confining one species at the interface and another at the surface, making it a good candidate for solar energy storage<sup>32,33</sup> below  $T_c$ . This work thus reveals the extraordinary physical properties of FE/manganite heterostructures, and represents an excellent example of the functionality that can result from combining different complex oxides.

We acknowledge primary support for this work from the Department of Energy, Office of Basic Energy Sciences, Division of Material Sciences and Engineering. Partial support was also provided by Los Alamos National Laboratory's Directed Research and Development Program. Los Alamos National Laboratory, an affirmative action equal opportunity employer, is operated by Los Alamos National Security, LLC, for the National Nuclear Security Administration of the US Department of Energy under Contract No. DE-AC52-06NA25396.

<sup>1</sup>J. F. Scott, *Science* **315**, 954 (2007).

<sup>2</sup>K. J. Choi, M. Biegalski, Y. L. Li, A. Sharan, J. Schubert, R. Uecker, P. Reiche, Y. B. Chen, X. Q. Pan, V. Gopalan *et al.*, *Science* **306**, 1005 (2004).

<sup>3</sup>N. A. Pertsev, A. G. Zembilgotov, and A. K. Tagantsev, *Phys. Rev. Lett.* **80**, 1988 (1998).

<sup>4</sup>V. B. Shirokov, Y. I. Yuzyuk, B. Dkhil, and V. V. Lemanov, *Phys. Rev. B* **79**, 144118 (2009).

<sup>5</sup>J. Junquera and P. Ghosez, *Nature (London)* **422**, 506 (2003).

<sup>6</sup>I. P. Batra, P. Wurfel, and B. D. Silverman, *Phys. Rev. B* **8**, 3257 (1973).

<sup>7</sup>H. N. Lee, H. M. Christen, M. F. Chisholm, C. M. Rouleau, and D. H. Lowndes, *Nature (London)* **433**, 395 (2005).

<sup>8</sup>J. E. Spanier, A. M. Kolpak, J. J. Urban, I. Grinberg, L. Ouyang, W. S. Yun, A. M. Rappe, and H. Park, *Nano Lett.* **6**, 735 (2006).

<sup>9</sup>See Supplemental Material at <http://link.aps.org/supplemental/10.1103/PhysRevB.88.020101> for additional information, includ-

ing the experimental setup and procedure, sample preparation, and a description of how the band offset was determined.

<sup>10</sup>H. Wen, P. Chen, M. P. Cosgriff, D. A. Walko, J. H. Lee, C. Adamo, R. D. Schaller, J. F. Ihlefeld, E. M. Dufresne, D. G. Schlom *et al.*, *Phys. Rev. Lett.* **110**, 037601 (2013).

<sup>11</sup>Y. M. Sheu, S. A. Trugman, Y.-S. Park, S. Lee, H. T. Yi, S.-W. Cheong, Q. X. Jia, A. J. Taylor, and R. P. Prasankumar, *Appl. Phys. Lett.* **100**, 242904 (2012).

<sup>12</sup>V. V. Lemanov, E. P. Smirnova, P. P. Syrnikov, and E. A. Tarakanov, *Phys. Rev. B* **54**, 3151 (1996).

<sup>13</sup>D. A. Tenne, A. Soukiassian, X. X. Xi, H. Choosuan, R. Guo, and A. S. Bhalla, *Phys. Rev. B* **70**, 174302 (2004).

<sup>14</sup>S. A. Denev, T. T. A. Lummen, E. Barnes, and G. Kumar, *J. Am. Ceram. Soc.* **94**, 2699 (2011).

<sup>15</sup>J. Bloch, J. G. Mihaychuk, and H. M. van Driel, *Phys. Rev. Lett.* **77**, 920 (1996).

<sup>16</sup>J. G. Mihaychuk, J. Bloch, Y. Liu, and H. M. van Driel, *Opt. Lett.* **20**, 2063 (1995).

- <sup>17</sup>X. Lu, R. Pasternak, H. Park, J. Qi, N. H. Tolk, A. Chatterjee, R. D. Schrimpf, and D. M. Fleetwood, *Phys. Rev. B* **78**, 155311 (2008).
- <sup>18</sup>S. Tinte, M. G. Stachiotti, S. R. Phillpot, M. Sepiarsky, D. Wolf, and R. L. Migoni, *J. Phys.: Condens. Matter* **16**, 3495 (2004).
- <sup>19</sup>S. Adikary and H. Chan, *Thin Solid Films* **424**, 70 (2003).
- <sup>20</sup>F. Pontes, E. Longo, E. Leite, and J. Varela, *Thin Solid Films* **386**, 91 (2001).
- <sup>21</sup>V. Ruckebauer, F. Hau, S. Lu, K. Yeung, C. Mak, and K. Wong, *Appl. Phys. A* **78**, 1049 (2004).
- <sup>22</sup>O. Lee, S. A. Harrington, A. Kursumovic, E. Defay, H. Wang, Z. Bi, C.-F. Tsai, L. Yan, Q. Jia, and J. L. MacManus-Driscoll, *Nano Lett.* **12**, 4311 (2012).
- <sup>23</sup>S.-T. Chang and J. Y. min Lee, *Appl. Phys. Lett.* **80**, 655 (2002).
- <sup>24</sup>F. J. Xia, Y. J. Fu, J. Yuan, H. Wu, Z. Xie, B. Xu, L. X. Cao, B. R. Zhao, and B. Y. Zhu, *J. Appl. Phys.* **110**, 103716 (2011).
- <sup>25</sup>R. Schafraneck, S. Payan, M. Maglione, and A. Klein, *Phys. Rev. B* **77**, 195310 (2008).
- <sup>26</sup>G. F. Dionne, *Magnetic Oxides* (Springer, New York, 2009).
- <sup>27</sup>M. Cardona, *Phys. Rev.* **140**, A651 (1965).
- <sup>28</sup>R. Thielsch, K. Kaemmer, and L. Schultz, *Thin Solid Films* **301**, 203 (1997).
- <sup>29</sup>H. Y. Tian, W. G. Luo, X. H. Pu, X. Y. He, P. S. Qiu, A. L. Ding, S. H. Yang, and D. Mo, *J. Phys.: Condens. Matter* **13**, 4065 (2001).
- <sup>30</sup>C. Samantaray, H. Sim, and H. Hwang, *Phys. B: Condens. Matter* **351**, 158 (2004).
- <sup>31</sup>F. M. Pontes, E. R. Leite, D. S. L. Pontes, E. Longo, E. M. S. Santos, S. Mergulhao, P. S. Pizani, J. F. Lanciotti, T. M. Boschi, and J. A. Varela, *J. Appl. Phys.* **91**, 5972 (2002).
- <sup>32</sup>J. Heber, *Nature (London)* **459**, 28 (2009).
- <sup>33</sup>H. Huang, *Nat. Photon.* **4**, 134 (2010).